J. Fluid Mech. (1995), *vol.* 286, *pp.* 277–290

Multi-mode models of flow and of solute dispersion in shallow water. Part 2. Logarithmic velocity profiles

By R. SMITH

Mathematical Sciences, Loughborough University of Technology, LE11 3TU, UK

(Received 1 July 1994 and in revised form 12 October 1994)

A two-mode model for velocity and solute concentration in shallow-water flows is derived which allows for departures from the logarithmic velocity profile and from vertically well-mixed concentrations. The modelling is tested against exact results for a buoyancy-driven transverse flow and for a modified logarithmic velocity profile.

1. Introduction

Certain features of shallow-water flow and solute dispersion cannot be represented in the simplest vertically averaged model equations. Amongst those features are the skewed flows and greatly enhanced transverse dispersion when different driving forces (pressure gradient, buoyancy, wind stress, Coriolis effects) are not aligned or when a single driving force is neither parallel nor perpendicular to the depth contours. Davies (1987) reviews the use of more than one mode to represent skewed flows in offshore waters. In Part 1 of this sequence of papers (Smith 1995) the multi-mode approach was extended to encompass solute dispersion. For the illustrative example of laminar flows it was demonstrated that a two-mode model accurately accounted for the differences in flow structure and in solute dispersion between Poiseuille (pressure-gradient driven) and Couette (surface-stress driven) flows.

In practical coastal engineering situations the flows are not laminar. So, the selection of modes made in Part 1, for constant-viscosity flows, would not be as efficient when the flows are turbulent. Accuracy would be lost or more than two modes would need to be computed. The purpose of the present paper is to derive and test a two-mode model appropriate for smooth-bed turbulent flows(with von-Kármán velocity profiles near the bed).

2. Legendre polynomial modes

In sigma coordinates (Phillips 1957), σ denotes the fractional distance between the bed ($\sigma = 0$) and the water surface ($\sigma = 1$). Guided by the work of Heaps (1972) but using the notation of Part 1, we use an idealized dimensionless shape $\hat{\kappa}(\sigma)$ of the eddy diffusivity to determine the concentration modes $\Psi^{(m)}(\sigma)$. In terms of the modes the concentration $c(x, y, \sigma, t)$ is represented

$$c = \sum_{m=0}^{\infty} c^{(m)}(x, y, t)\Psi^{(m)}(\sigma). \tag{2.1}$$

The actual modelling for the eddy diffusivity $\kappa(x, y, \sigma, t)$ can deviate in shape from the ideal (see §6). However, we can anticipate that the more appropriate the choice of $\hat{\kappa}(\sigma)$ the more rapid the decay of successive concentration amplitudes $c^{(0)}$, $c^{(1)}$, ... and the better the accuracy of a truncated representation.

For turbulent open channel flows the classical von Kármán shape for the eddy diffusivity and eddy viscosity profiles is a parabola

$$\hat{\kappa}(\sigma) = \hat{\nu}(\sigma) = (1-\sigma)(\sigma+\sigma_*), \tag{2.2}$$

where σ_* is the extremely small dimensionless roughness height (about 0.0001). With terms of order σ_* neglected, the diffusion eigenmodes are rescaled Legendre Polynomials

$$\Psi^{(0)} = 1,\ \Psi^{(1)} = \sqrt{3}\,(2\sigma-1),\ \Psi^{(m)} = (2m+1)^{1/2}\,P_m(2\sigma-1),\ \lambda^{(m)} = m(m+1). \tag{2.3a-d}$$

The eigenvalues $\lambda^{(m)}$ are dimensionless response rates. The evolution equation satisfied by $c^{(m)}(x, y, t)$ is the $\Psi^{(m)}$ component of the concentration transport equation (Part 1, (4.3)).

The two horizontal velocity components $u(x, y, \sigma, t)$ and $v(x, y, \sigma, t)$ have the representations

$$u = \sum_{m=0}^{\infty} u^{(m)}(x, y, t)\Phi^{(m)}(\sigma), \quad v = \sum_{m=0}^{\infty} v^{(m)}(x, y, t)\Phi^{(m)}(\sigma), \tag{2.4a, b}$$

where $\Phi^{(m)}(\sigma)$ are the velocity modes. Although $\hat{\kappa}(\sigma)$ and $\hat{\nu}(\sigma)$ are equal, the different bed boundary conditions of zero concentration flux and of no slip, make the concentration and velocity modes ($\Psi^{(m)}$, $\lambda^{(m)}$) and ($\Phi^{(m)}$, $\mu^{(m)}$) unequal.

To represent the velocity eigenmodes we introduce the small parameter ε (about 1/9)

$$\varepsilon = -1/\ln\sigma_*, \quad \sigma_* = \exp(-1/\varepsilon). \tag{2.5a, b}$$

Correct to the stated order in ε the velocity eigenmodes are

$$\Phi^{(0)} = \left\{1 + \varepsilon - \tfrac{1}{2}\varepsilon^2 + \ldots\right\}\left\{[1 + \varepsilon\ln(\sigma+\sigma_*)] + \varepsilon^2\sum_{j=1}^{\infty}\frac{(2j+1)}{j^2(j+1)^2}\left[1 + (-1)^{j-1}P_j(2\sigma-1)\right] + \ldots\right\}, \tag{2.6a}$$

$$\Phi^{(1)} = \sqrt{3}\left\{1 + \tfrac{7}{3}\varepsilon + \ldots\right\}\left\{(2\sigma-1)\left[1 + \varepsilon\ln(\sigma+\sigma_*)\right] - 2\varepsilon\sigma + \ldots\right\}, \tag{2.6b}$$

$$\Phi^{(m)} = (2m+1)^{1/2}\left\{1 + \frac{\varepsilon}{2m+1} + 2\varepsilon\sum_{j=1}^{2m}\frac{(-1)^j}{j} + 2\varepsilon\sum_{j=0}^{m-1}\frac{(2j+1)}{(m-j)(m+j+1)} + \ldots\right\} \times \left\{P_m(2\sigma-1)\left[1 + \varepsilon\ln(\sigma-\sigma_*)\right] + 2\varepsilon\sum_{j=0}^{m-1}\frac{(2j+1)}{(m-j)(m+j+1)}\left[(-1)^{m-j}P_j(2\sigma-1) - P_m(2\sigma-1)\right] + \ldots\right\}, \tag{2.6c}$$

$$\mu^{(m)} = m(m+1) + \varepsilon(2m+1) + \ldots. \tag{2.6d}$$

The logarithms are associated with the no-slip boundary condition at the bed. The evolution equations satisfied by $u^{(m)}$, $v^{(m)}$ are the $\Phi^{(m)}$ components of the horizontal momentum equations (Part 1, (3.4)).

To a first approximation the sigma coordinate system accounts directly for the vertical motion associated both with non-uniformly in the bed level $z = -h(x, y)$ and with variations in the free surface position $z = \zeta(x, y, t)$. A full representation of the vertical motion (Part 1, (2.3), (3.2)) involves auxiliary modes $\omega^{(m)}$:

$$\omega^{(0)} = -\left(\varepsilon + \varepsilon^2\right)\sigma \ln(\sigma + \sigma_*) + \frac{\varepsilon^2}{2}\sum_{j=1}^{\infty} \frac{(-1)^j}{j^2(j+1)^2}\left[P_{j+1}(2\sigma - 1) - P_{j-1}(2\sigma - 1)\right] + \ldots, \tag{2.7a}$$

$$\omega^{(1)} = \sqrt{3}\left\{(-\sigma^2 + \sigma)\left[1 + \varepsilon \ln(\sigma + \sigma_*) + \varepsilon\tfrac{5}{6}\right] + \ldots\right\}, \tag{2.7b}$$

$$\begin{aligned}\omega^{(m)} = &-\frac{[P_{m+1}(2\sigma - 1) - P_{m-1}(2\sigma - 1)]}{2(2m+1)^{1/2}}\left[1 + \varepsilon \ln(\sigma + \sigma_*)\right.\\ &\left. - \frac{\varepsilon}{m+1} + \frac{\varepsilon}{2m+1} + 2\varepsilon\sum_{j=1}^{2m}\frac{(-1)^{j-1}}{j}\right]\\ &- \frac{\varepsilon(2m+1)^{1/2}}{2m(m+1)}\left[P_m(2\sigma - 1) - P_{m-1}(2\sigma - 1) + 2(-1)^m(\sigma - 1)\right]\\ &+ \varepsilon(2m+1)^{1/2}\sum_{j=1}^{m-1}\frac{(-1)^{m-j+1}}{(m-j)(m+j+1)}\left[P_{j+1}(2\sigma - 1) - P_{j-1}(2\sigma - 1)\right] + \ldots.\end{aligned} \tag{2.7c}$$

3. Mass, momentum and concentration equations

In a truncation involving just the $m = 0$ and $m = 1$ velocity modes the vertically integrated mass conservation equation (Part 1, (3.3)) becomes

$$\frac{\partial \zeta}{\partial t} + \left[1 - \frac{\varepsilon^2}{2}\right]\left\{\frac{\partial}{\partial x}(Hu^{(0)}) + \frac{\partial}{\partial y}(Hv^{(0)})\right\} - \varepsilon\frac{\sqrt{3}}{2}\left\{\frac{\partial}{\partial x}(Hu^{(1)}) + \frac{\partial}{\partial y}(Hv^{(1)})\right\} = H\int_0^1 Q\,\mathrm{d}\sigma, \tag{3.1a}$$

where

$$H = \zeta + h, \tag{3.1b}$$

and $Q(x, y, \sigma, t)$ represents the volume discharge rate of water at any sources in the flow. In the limit as ε tends to zero this becomes the classical (vertically averaged) mass conservation equation (Lamb 1945, Chapter 8).

For the viscosity we pose the decomposition

$$\nu = N\hat{\nu} + \nu' \qquad \text{where} \qquad \int_0^1 \frac{\nu'}{(\sigma + \sigma_*)^2}\mathrm{d}\sigma = 0. \tag{3.2}$$

Thus, the representative value N is strongly weighted by values close to the bed (i.e. ν' is extremely small near the bed).

In a two-mode truncation the horizontal momentum equations (Part 1, (3.4*a*,*b*)) are

$$\frac{\partial}{\partial t}(Hu^{(0)}) + \left[1+\varepsilon^2\frac{3}{2}\right]\left\{\frac{\partial}{\partial x}(Hu^{(0)^2}) + \frac{\partial}{\partial y}(Hv^{(0)}u^{(0)})\right\}$$
$$+ \varepsilon\frac{\sqrt{3}}{2}\left\{2\frac{\partial}{\partial x}(Hu^{(0)}u^{(1)}) + \frac{\partial}{\partial y}(Hv^{(0)}u^{(1)} + Hv^{(1)}u^{(0)})\right\}$$
$$+ \left[1-\frac{\varepsilon}{3}\right]\left\{\frac{\partial}{\partial x}(Hu^{(1)^2}) + \frac{\partial}{\partial y}(Hv^{(1)}u^{(1)})\right\} - \varepsilon^2\left\{\frac{\partial}{\partial x}(Hu^{(0)}) + \frac{\partial}{\partial y}(Hv^{(0)})\right\}u^{(0)}$$
$$- \varepsilon\frac{\sqrt{3}}{2}\left\{\frac{\partial}{\partial x}(Hu^{(1)}) + \frac{\partial}{\partial y}(Hv^{(1)})\right\}u^{(0)}$$
$$+ \frac{\varepsilon}{2}\left\{\frac{\partial}{\partial x}(Hu^{(1)}) + \frac{\partial}{\partial y}(Hv^{(1)})\right\}u^{(1)} - Hfv^{(0)}$$
$$= H\int_0^1 M_1\Phi^{(0)}\mathrm{d}\sigma - Hu^{(0)}\int_0^1 Q\Phi^{(0)^2}\mathrm{d}\sigma - Hu^{(1)}\int_0^1 Q\Phi^{(0)}\Phi^{(1)}\mathrm{d}\sigma$$
$$- \left[1-\frac{\varepsilon^2}{2}\right]H\left\{\frac{1}{\rho_0}\frac{\partial P}{\partial x} + g\frac{\partial\zeta}{\partial x}\right\} - \left[\frac{1}{2} - \frac{\varepsilon}{4} - \frac{3}{8}\varepsilon^2\right]\alpha gH^2\frac{\partial c^{(0)}}{\partial x}$$
$$- \sqrt{3}\left[\frac{1}{6} + \frac{\varepsilon}{36}\right]\alpha gH^2\frac{\partial c^{(1)}}{\partial x} - \sqrt{3}\left[\frac{1}{3} - \varepsilon\frac{5}{18}\right]\alpha gH\frac{\partial H}{\partial x}c^{(1)}$$
$$+ \left[1+\varepsilon-\frac{\varepsilon^2}{2}\right]\frac{\tau_1}{\rho_0} - \varepsilon[1+\varepsilon]\frac{N}{H}u^{(0)} - \varepsilon\frac{u^{(1)}}{H}2\sqrt{3}\int_0^1\frac{v'}{\sigma+\sigma_*}\mathrm{d}\sigma, \qquad (3.3a)$$

$$\frac{\partial}{\partial t}(Hv^{(0)}) + \left[1+\varepsilon^2\frac{3}{2}\right]\left\{\frac{\partial}{\partial x}(Hu^{(0)}v^{(0)}) + \frac{\partial}{\partial y}(Hv^{(0)^2})\right\}$$
$$+ \varepsilon\frac{\sqrt{3}}{2}\left\{\frac{\partial}{\partial x}(Hu^{(0)}v^{(1)} + Hu^{(1)}v^{(0)}) + 2\frac{\partial}{\partial y}(Hv^{(0)}v^{(1)})\right\}$$
$$+ \left[1-\frac{\varepsilon}{3}\right]\left\{\frac{\partial}{\partial x}(Hu^{(1)}v^{(1)}) + \frac{\partial}{\partial y}(Hv^{(1)^2})\right\} - \varepsilon^2\left\{\frac{\partial}{\partial x}(Hu^{(0)}) + \frac{\partial}{\partial y}(Hv^{(0)})\right\}v^{(0)}$$
$$- \varepsilon\frac{\sqrt{3}}{2}\left\{\frac{\partial}{\partial x}(Hu^{(1)}) + \frac{\partial}{\partial y}(Hv^{(1)})\right\}v^{(0)}$$
$$+ \frac{\varepsilon}{2}\left\{\frac{\partial}{\partial x}(Hu^{(1)}) + \frac{\partial}{\partial y}(Hv^{(1)})\right\}v^{(1)} + Hfu^{(0)}$$
$$= H\int_0^1 M_2\Phi^{(0)}\mathrm{d}\sigma - Hu^{(0)}\int_0^1 Q\Phi^{(0)^2}\mathrm{d}\sigma - Hu^{(1)}\int_0^1 Q\Phi^{(0)}\Phi^{(1)}\mathrm{d}\sigma$$
$$- \left[1-\frac{\varepsilon^2}{2}\right]H\left\{\frac{1}{\rho_0}\frac{\partial P}{\partial y} + g\frac{\partial\zeta}{\partial y}\right\} - \left[\frac{1}{2} - \frac{\varepsilon}{4} - \frac{3}{8}\varepsilon^2\right]\alpha gH^2\frac{\partial c^{(0)}}{\partial y}$$
$$- \sqrt{3}\left[\frac{1}{6} + \frac{\varepsilon}{36}\right]\alpha gH^2\frac{\partial c^{(1)}}{\partial y} - \sqrt{3}\left[\frac{1}{3} - \varepsilon\frac{5}{18}\right]\alpha gH\frac{\partial H}{\partial y}c^{(1)}$$
$$+ \left[1+\varepsilon-\frac{\varepsilon^2}{2}\right]\frac{\tau_2}{\rho_0} - \varepsilon\ [1+\varepsilon]\ \frac{N}{H}v^{(0)} - \varepsilon\frac{v^{(1)}}{H}2\sqrt{3}\int_0^1\ \frac{v'}{\sigma+\sigma_*}\mathrm{d}\sigma, \qquad (3.3b)$$

$$\frac{\partial}{\partial t}(Hu^{(1)}) + \varepsilon\frac{\sqrt{3}}{2}\left\{\frac{\partial}{\partial x}(Hu^{(0)^2}) + \frac{\partial}{\partial y}(Hv^{(0)}u^{(0)})\right\}$$
$$+ \left[1-\frac{\varepsilon}{3}\right]\left\{2\frac{\partial}{\partial x}(Hu^{(0)}u^{(1)}) + \frac{\partial}{\partial y}(Hv^{(0)}u^{(1)} + Hv^{(1)}u^{(0)})\right\}$$
$$- \varepsilon\frac{\sqrt{3}}{2}\left\{\frac{\partial}{\partial x}(Hu^{(0)}) + \frac{\partial}{\partial y}(Hv^{(0)})\right\}u^{(0)} - \left[1+\frac{\varepsilon}{6}\right]\left\{\frac{\partial}{\partial x}(Hu^{(1)}) + \frac{\partial}{\partial y}(Hv^{(1)})\right\}u^{(0)}$$
$$+ \frac{\varepsilon}{6}\left\{\frac{\partial}{\partial x}(Hu^{(0)}) + \frac{\partial}{\partial y}(Hv^{(0)})\right\}u^{(1)} - \varepsilon\frac{\sqrt{3}}{4}\left\{\frac{\partial}{\partial x}(Hu^{(1)}) + \frac{\partial}{\partial y}(Hv^{(1)})\right\}u^{(1)} - Hfv^{(1)}$$
$$= H\int_0^1 M_1\Phi^{(1)}\mathrm{d}\sigma - Hu^{(0)}\int_0^1 Q\Phi^{(0)}\Phi^{(1)}\mathrm{d}\sigma - Hu^{(1)}\int_0^1 Q\Phi^{(1)^2}\mathrm{d}\sigma$$
$$+ \varepsilon\frac{\sqrt{3}}{2}H\left\{\frac{1}{\rho_0}\frac{\partial P}{\partial x} + g\frac{\partial\zeta}{\partial x}\right\} + \sqrt{3}\left[\frac{1}{6}+\frac{\varepsilon}{4}\right]\alpha gH^2\frac{\partial c^{(0)}}{\partial x} + \varepsilon\frac{3}{8}\alpha gH^2\frac{\partial c^{(1)}}{\partial x}$$
$$+ \left[\frac{1}{2}-\varepsilon\frac{37}{24}\right]\alpha gH\frac{\partial H}{\partial x}c^{(1)} + \sqrt{3}\left[1+\frac{\varepsilon}{3}\right]\frac{\tau_1}{\rho_0} - \varepsilon\frac{u^{(0)}}{H}2\sqrt{3}\int_0^1\frac{v'}{\sigma+\sigma_*}\mathrm{d}\sigma$$
$$- \frac{u^{(1)}}{H}\left\{2N + 3\varepsilon N + 12\int_0^1 v'\mathrm{d}\sigma - 12\varepsilon\int_0^1 v'\left[\frac{1}{\sigma+\sigma_*} - \frac{8}{3} - 2\ln(\sigma+\sigma_*)\right]\mathrm{d}\sigma\right\}, \quad (3.3c)$$

$$\frac{\partial}{\partial t}(Hv^{(1)}) + \varepsilon\frac{\sqrt{3}}{2}\left\{\frac{\partial}{\partial x}(Hu^{(0)}v^{(0)}) + \frac{\partial}{\partial y}(Hv^{(0)^2})\right\}$$
$$+ \left[1-\frac{\varepsilon}{3}\right]\left\{\frac{\partial}{\partial x}(Hu^{(0)}v^{(1)} + Hu^{(1)}v^{(0)}) + 2\frac{\partial}{\partial y}(Hv^{(0)}v^{(1)})\right\}$$
$$- \varepsilon\frac{\sqrt{3}}{2}\left\{\frac{\partial}{\partial x}(Hu^{(0)}) + \frac{\partial}{\partial y}(Hv^{(0)})\right\}v^{(0)} - \left[1+\frac{\varepsilon}{6}\right]\left\{\frac{\partial}{\partial x}(Hu^{(1)}) + \frac{\partial}{\partial y}(Hv^{(1)})\right\}v^{(0)}$$
$$+ \frac{\varepsilon}{6}\left\{\frac{\partial}{\partial x}(Hu^{(0)}) + \frac{\partial}{\partial y}(Hv^{(0)})\right\}v^{(1)} - \varepsilon\frac{\sqrt{3}}{4}\left\{\frac{\partial}{\partial x}(Hu^{(1)}) + \frac{\partial}{\partial y}(Hv^{(1)})\right\}v^{(1)} + Hfu^{(1)}$$
$$= H\int_0^1 M_2\Phi^{(1)}\mathrm{d}\sigma - Hv^{(0)}\int_0^1 Q\Phi^{(0)}\Phi^{(1)}\mathrm{d}\sigma - Hv^{(1)}\int_0^1 Q\Phi^{(1)^2}\mathrm{d}\sigma$$
$$+ \varepsilon\frac{\sqrt{3}}{2}H\left\{\frac{1}{\rho_0}\frac{\partial P}{\partial y} + g\frac{\partial\zeta}{\partial y}\right\} + \sqrt{3}\left[\frac{1}{6}+\frac{\varepsilon}{4}\right]\alpha gH^2\frac{\partial c^{(0)}}{\partial y} + \varepsilon\frac{3}{8}\alpha gH^2\frac{\partial c^{(1)}}{\partial y}$$
$$+ \left[\frac{1}{2}-\varepsilon\frac{37}{24}\right]\alpha gH\frac{\partial H}{\partial y}c^{(1)} + \sqrt{3}\left[1+\frac{\varepsilon}{3}\right]\frac{\tau_2}{\rho_0} - \varepsilon\frac{v^{(0)}}{H}2\sqrt{3}\int_0^1\frac{v'}{\sigma+\sigma_*}\mathrm{d}\sigma$$
$$- \frac{v^{(1)}}{H}\left\{2N + 3\varepsilon N + 12\int_0^1 v'\mathrm{d}\sigma - 12\varepsilon\int_0^1 v'\left[\frac{1}{\sigma+\sigma_*} - \frac{8}{3} - 2\ln(\sigma+\sigma_*)\right]\mathrm{d}\sigma\right\}. \quad (3.3d)$$

To facilitate practical applications, numerous complications have been accounted for: f is the Coriolis frequency, M_1, M_2 are momenta associated with any body forces or discharges, P is the atmospheric pressure, ρ_0 is a reference water density, $\alpha\rho_0 c$ is the density perturbation caused by the solute, and τ_1, τ_2 are surface wind stresses. The coefficients are correct to the stated order in ε.

The eddy viscosity N-terms in equations (3.3 *c,d*) for $u^{(1)}$ and $v^{(1)}$ are order ε larger than the N-terms in equations (3.3 *a,b*) for $u^{(0)}$ and $v^{(0)}$. The pressure gradient terms

exhibit the converse disparity. If the force balance were principally between bottom drag and pressure gradient, then $u^{(1)}$, $v^{(1)}$ would be order ε^2 smaller than $u^{(0)}$, $v^{(0)}$. When we ignore $u^{(1)}$, $v^{(1)}$ the non-visocity coefficients only differ by order ε^2 from the coefficients in the shallow-water approximation (Lamb 1945, Chapter 8). To minimize errors, Falconer (1976) advocates the retention of such correction factors for the non-uniform velocity profile in practical prediction methods.

The two-mode truncation of the concentration equations (Part 1, (4.3)) is

$$\begin{aligned}
&\frac{\partial}{\partial t}(Hc^{(0)}) + \left[1 - \frac{\varepsilon^2}{2}\right]\left\{\frac{\partial}{\partial x}(Hu^{(0)}c^{(0)}) + \frac{\partial}{\partial y}(Hv^{(0)}c^{(0)})\right\} \\
&+ \varepsilon\frac{\sqrt{3}}{2}\left[1 + \frac{3}{2}\varepsilon\right]\left\{\frac{\partial}{\partial x}(Hu^{(0)}c^{(1)}) + \frac{\partial}{\partial y}(Hv^{(0)}c^{(1)})\right\} \\
&- \varepsilon\frac{\sqrt{3}}{2}\left\{\frac{\partial}{\partial x}(Hu^{(1)}c^{(0)}) + \frac{\partial}{\partial y}(Hv^{(1)}c^{(0)})\right\} + \left\{\frac{\partial}{\partial x}(Hu^{(1)}c^{(1)}) + \frac{\partial}{\partial y}(Hv^{(1)}c^{(1)})\right\} \\
&= H\int_0^1 (q - c^{(0)}Q)\mathrm{d}\sigma - Hc^{(1)}\int_0^1 \sqrt{3}(2\sigma - 1)Q\mathrm{d}\sigma \\
&+ \frac{\partial}{\partial x}\left(H\int_0^1 K\ \mathrm{d}\sigma\ \frac{\partial c^{(0)}}{\partial x}\right) + \frac{\partial}{\partial x}\left(H\int_0^1 \sqrt{3}(2\sigma - 1)K\ \mathrm{d}\sigma\ \frac{\partial c^{(1)}}{\partial x}\right) \\
&+ \frac{\partial}{\partial y}\left(H\int_0^1 K\ \mathrm{d}\sigma\ \frac{\partial c^{(0)}}{\partial y}\right) + \frac{\partial}{\partial y}\left(H\int_0^1 \sqrt{3}(2\sigma - 1)K\ \mathrm{d}\sigma\ \frac{\partial c^{(1)}}{\partial y}\right), \qquad (3.4a)
\end{aligned}$$

$$\begin{aligned}
&\frac{\partial}{\partial t}(Hc^{(1)}) + \varepsilon\frac{\sqrt{3}}{2}\left[1 + \frac{3}{2}\varepsilon\right]\left\{\frac{\partial}{\partial x}(Hu^{(0)}c^{(0)}) + \frac{\partial}{\partial y}(Hv^{(0)}c^{(0)}\right\} \\
&+ \left[1 - \frac{\varepsilon}{2} - \frac{11}{12}\varepsilon^2\right]\left\{\frac{\partial}{\partial x}(Hu^{(0)}c^{(1)}) + \frac{\partial}{\partial y}(Hv^{(0)}c^{(1)})\right\} \\
&+ \left\{\frac{\partial}{\partial x}(Hu^{(1)}c^{(0)}) + \frac{\partial}{\partial y}(Hv^{(1)}c^{(0)})\right\} \\
&+ \varepsilon 2\sqrt{3}\left\{\frac{\partial}{\partial x}(Hu^{(1)}c^{(1)}) + \frac{\partial}{\partial y}(Hv^{(1)}c^{(1)})\right\} \\
&- \varepsilon\frac{\sqrt{3}}{2}\left\{\frac{\partial}{\partial x}(Hu^{(0)}) + \frac{\partial}{\partial y}(Hv^{(0)})\right\}c^{(0)} - \left\{\frac{\partial}{\partial x}(Hu^{(1)}) + \frac{\partial}{\partial y}(Hv^{(1)})\right\}c^{(0)} \\
&+ \frac{\varepsilon}{6}\left[1 + \frac{\varepsilon}{24}\right]\left\{\frac{\partial}{\partial x}(Hu^{(0)}) + \frac{\partial}{\partial y}(Hv^{(0)})\right\}c^{(1)} \\
&- \varepsilon\frac{\sqrt{3}}{4}\left\{\frac{\partial}{\partial x}(Hu^{(1)}) + \frac{\partial}{\partial y}(Hv^{(1)})\right\}c^{(1)} \\
&= H\int_0^1 \sqrt{3}(2\sigma - 1)(q - c^{(0)}Q)\mathrm{d}\sigma - Hc^{(1)}\int_0^1 3(2\sigma - 1)^2 Q\ \mathrm{d}\sigma \\
&- 12\frac{c^{(1)}}{H}\int_0^1 \kappa\ \mathrm{d}\sigma. \qquad (3.4b)
\end{aligned}$$

Here $q(x, y, \sigma, t)$ is the source strength. Again, the coefficients are correct to the stated order in ε. In equation (3.4*b*) the K-integral terms representing horizontal

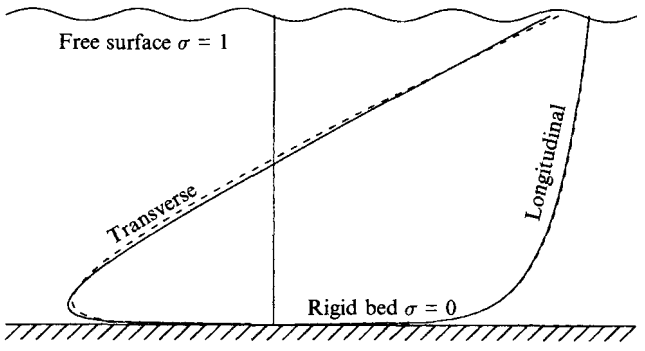

FIGURE 1. Pressure-driven longitudinal velocity and buoyancy-driven transverse velocity (——) for turbulent open-channel flow, compared with the two-mode approximations (- - - -).

diffusion have been neglected on the premise the square of the depth-to-horizontal ratio of length scales is very small. There are no shear dispersion coefficients in equations (3.4*a*,*b*). It is the interaction between $c^{(0)}$ and $c^{(1)}$ that gives rise to the dispersion process (Part 1, Appendix).

4. Test of longitudinal velocity and dispersion

As in the laminar tests (Part 1, §§6, 7), we restrict attention to steady uni-directional flows in water of constant depth with no buoyancy or rotation effects and to discharges with negligible volume or momentum. For the eddy viscosity and diffusivities we use the model (Fischer 1973):

$$\nu = \kappa = k\, u_* H(1-\sigma)(\sigma+\sigma_*)\,, \qquad K = \tfrac{1}{2}\, k\, u_* H\, \sigma^{1/3} \tag{4.1a,b}$$

where k is von Kármán's constant (about 0.4) and u_* is the friction velocity.

For a steady pressure-driven flow, the exact velocity has a logarithmic profile

$$u = -\frac{H}{\varepsilon k\, u_*}\left\{\frac{1}{\rho_0}\frac{\partial P}{\partial x} + g\frac{\partial \zeta}{\partial x}\right\}[1+\varepsilon \ln(\sigma+\sigma_*)] \text{ with } u_*^2 = -H\left\{\frac{1}{\rho_0}\frac{\partial P}{\partial x} + g\frac{\partial \zeta}{\partial x}\right\}. \tag{4.2a,b}$$

In the two-mode approximation, (3.3*a*–*d*), the steady solutions are

$$u^{(0)} = -\frac{[1-\varepsilon^2/2]}{\varepsilon[1+\varepsilon]}\,\frac{H}{k\, u_*}\left\{\frac{1}{\rho_0}\frac{\partial P}{\partial x} + g\frac{\partial \zeta}{\partial x}\right\}, \tag{4.3a}$$

$$u^{(1)} = \frac{\varepsilon\sqrt{3}}{2[2+3\varepsilon]}\,\frac{H}{k\, u_*}\left\{\frac{1}{\rho_0}\frac{\partial P}{\partial x} + g\frac{\partial \zeta}{\partial x}\right\}. \tag{4.3b}$$

Figure 1 compares the dimensionless velocity profiles

$$[1+\varepsilon\ln(\sigma+\sigma_*)] \text{ and } \frac{[1-\varepsilon^2/2]}{1+\varepsilon}\,\Phi^{(0)} - \frac{\sqrt{3}\varepsilon^2}{2[2+3\varepsilon]}\,\Phi^{(1)}, \tag{4.4a,b}$$

with $\Phi^{(0)}$, $\Phi^{(1)}$ given by the truncated formulae (2.6*a*,*b*) and with

$$\varepsilon = 1/9. \tag{4.5}$$

The small error exhibits the two zero crossings associated with the dominant neglected $m = 2$ mode.

In view of the truncation of the formulae (2.6*a*,*b*) for the eigenmodes $\Phi^{(0)}$, $\Phi^{(1)}$ and

the truncation of the coefficients in equations (3.3*a*,*c*), the expression (4.4*b*) is formally equivalent to

$$1+\varepsilon\ln(\sigma+\sigma_*)+\varepsilon^2\left\{\sum_{j=2}^{\infty}\frac{(2j+1)}{j^2(j+1)^2}(-1)^{j-1}P_j(2\sigma-1)-\frac{\varepsilon}{4}\ln(\sigma+\sigma_*)\right\}+\ldots. \quad (4.6)$$

This makes explicit the size ($5\varepsilon^2/36$) and shape $P_2(2\sigma-1)$ of the error. However, ε is not arbitrarily small and equations (4.4*b*), (4.6) are not identical. To test the actual errors it is appropriate to use the awkward full expression (4.4*b*) and not the neater formal approximation (4.6). The exact result for the asymptotic centroid velocity is

$$\bar{u}=-\frac{H}{\varepsilon k\, u_*}\left\{\frac{1}{\rho_0}\frac{\partial P}{\partial x}+g\frac{\partial\zeta}{\partial x}\right\}[1-\varepsilon]. \quad (4.7)$$

When $c^{(1)}$ has decayed, the natural velocity for $c^{(0)}$ in equation (3.4*a*) is

$$[1-\varepsilon^2/2]u^{(0)}-\varepsilon\frac{\sqrt{3}}{2}u^{(1)}. \quad (4.8)$$

If we substitute the values (4.3*a*,*b*) for $u^{(0}$ and $u^{(1)}$ we obtain the expression

$$-\frac{H}{\varepsilon\, k\, u_*}\left\{\frac{1}{\rho_0}\frac{\partial P}{\partial x}+g\frac{\partial\zeta}{\partial x}\right\}\left\{\frac{[1-\varepsilon^2/2]^2}{1+\varepsilon}+\frac{3\varepsilon^3}{4[2+3\varepsilon]}\right\}. \quad (4.9)$$

The fractional difference between equations (4.7) and (4.9) is formally of order ε^3 and numerically of size 0.0005 for $\varepsilon=1/9$.

Going beyond the standard shear dispersion models (Taylor 1953; Elder 1959) we consider the centroid displacement $G(\sigma')+G(\sigma)$ relating to the release height σ' and observation height σ. A Legendre polynomial series (Smith 1982, (9.7)) for the exact centroid displacement function is

$$G(\sigma)=-\frac{H^2}{k^2u_*^2}\left\{\frac{1}{\rho_0}\frac{\partial P}{\partial x}+g\frac{\partial\zeta}{\partial x}\right\}\sum_{j=1}^{\infty}\frac{(-1)^{j-1}(2j+1)}{j^2(j+1)^2}P_j(2\sigma-1). \quad (4.10)$$

For the two-mode model, the approximation for G is (Part 1, (A9)):

$$G=\frac{H}{2k\, u_*}\left[\varepsilon\frac{\sqrt{3}}{2}\left(1+\frac{3}{2}\varepsilon\right)u^{(0)}+u^{(1)}\right]\sqrt{3}(2\sigma-1). \quad (4.11)$$

The results (4.3*a*,*b*) for $u^{(0)}$, $u^{(1)}$ allow us to re-write this approximation:

$$G=-\frac{H}{k^2u_*^2}\left\{\frac{1}{\rho_0}\frac{\partial P}{\partial x}+g\frac{\partial\zeta}{\partial x}\right\}\left\{\frac{(1+3\varepsilon/2)(1-\varepsilon^2/2)}{1+\varepsilon}-\frac{\varepsilon}{2+3\varepsilon}\right\}\frac{3}{4}(2\sigma-1). \quad (4.12)$$

Figure 2 compares the shapes of the exact of approximate centroid displacement functions (4.10), (4.12).

Elder (1959) gives the longitudinal shear dispersion coefficient for logarithmic open-channel flow:

$$D=0.40411\left(\frac{H}{k\, u_*}\right)^3\left\{\frac{1}{\rho_0}\frac{\partial P}{\partial x}+g\frac{\partial\zeta}{\partial x}\right\}^2. \quad (4.13)$$

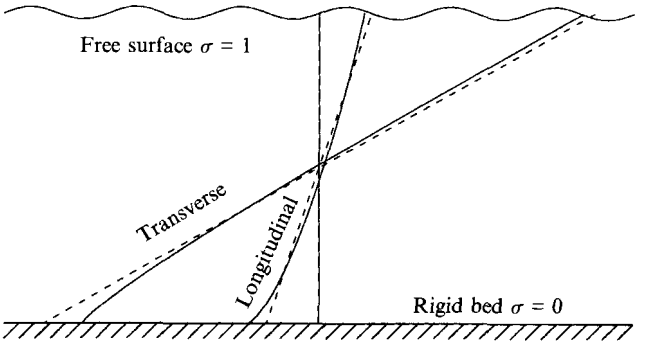

FIGURE 2. Shapes of the centroid displacement functions (——) and the two-mode approximations (- - - -) for pressure-driven longitudinal and buoyancy-driven transverse turbulent open-channel flows.

For the two-mode model the approximation for D is (Part1, (A11)):

$$D = \left[\varepsilon\frac{\sqrt{3}}{2}\left(1+\frac{3}{2}\varepsilon\right)u^{(0)} + u^{(1)}\right]^2 \frac{H}{k\,u_*}. \tag{4.14}$$

If we substitute for $u^{(0)}$, $u^{(1)}$, we obtain the approximation

$$D = \frac{3}{8}\left\{\frac{(1+3\varepsilon/2)(1-\varepsilon^2/2)}{1+\varepsilon} - \frac{\varepsilon}{2+3\varepsilon}\right\}^2 \left(\frac{H}{k\,u_*}\right)^3 \left\{\frac{1}{\rho_0}\frac{\partial P}{\partial x} + g\frac{\partial \zeta}{\partial x}\right\}^2. \tag{4.15}$$

For $\varepsilon = 1/9$ the numerical factor in the approximation (4.15) is 0.3719. Thus, the error in the shear dispersion coefficient is 8%. (This would correspond to an over estimate of 4% in the peak concentration.)

Again going beyond the standard shear dispersion models, we consider the deficit variance (Chatwin 1970)

$$2\overline{G^2} = 0.3835\left(\frac{H}{k\,u_*}\right)^4 \left\{\frac{1}{\rho_0}\frac{\partial P}{\partial x} + g\frac{\partial \zeta}{\partial x}\right\}^2. \tag{4.16}$$

From the two-mode result (4.12) we obtain the approximation

$$\frac{3}{8}\left\{\frac{(1+3\varepsilon/2)(1-\varepsilon^2/2)}{1+\varepsilon} - \frac{\varepsilon}{2+3\varepsilon}\right\}^2 \left(\frac{H}{k\,u_*}\right)^4 \left\{\frac{1}{\rho_0}\frac{\partial P}{\partial x} + g\frac{\partial \zeta}{\partial x}\right\}^2. \tag{4.17}$$

It happens that the numerical coefficient is the same as in equation (4.15), with the value 0.3719 when $\varepsilon = 1/9$. The error is only 3%.

5. Test of the transverse flow and dispersion

In the principal flow direction the $m = 0$ and $m = 1$ modes are both available to contribute to accurate representations of the flow and of the concentration. However, in the transverse direction the presence of side walls (y = constant) would enforce zero vertically integrated flow of water:

$$\left[1 - \frac{\varepsilon^2}{2}\right] v^{(0)} - \varepsilon\frac{\sqrt{3}}{2}v^{(1)} = 0 \tag{5.1}$$

(cf. equation (3.1*a*)). Thus, in the representation of the transverse flow we have lost one degree of freedom:

$$v(x,y,\sigma,t) = v^{(1)}(x,y,t)\left\{\frac{\varepsilon\sqrt{3}}{[2-\varepsilon^2]}\Phi^{(0)}(\sigma) + \Phi^{(1)}(\sigma)\right\}. \tag{5.2}$$

To test the accuracy of this representation and of the associated transverse shear dispersion, we consider the effect of buoyancy far downstream of a continuous discharge in a steady flow.

Sufficiently far downstream the dominant terms in the two-mode transverse momentum equations (3.3*b*,*d*) are

$$0 = -\left[1-\frac{\varepsilon^2}{2}\right] g\frac{\partial\zeta}{\partial y} - \left[\frac{1}{2}-\frac{\varepsilon}{4}-\frac{3}{8}\varepsilon^2\right]\alpha g H\frac{\partial c^{(0)}}{\partial y} - \frac{\varepsilon^2[1+\varepsilon]\sqrt{3}v^{(1)}k\ u_*}{[2-\varepsilon^2]\ H}, \tag{5.3a}$$

$$0 = \varepsilon\frac{\sqrt{3}}{2}g\frac{\partial\zeta}{\partial y} + \frac{\sqrt{3}}{6}\left[1+\varepsilon\frac{3}{2}\right]\alpha g H\ \frac{\partial c^{(0)}}{\partial y} - [2+3\varepsilon]\ \frac{v^{(1)}k\ u_*}{H}. \tag{5.3b}$$

The physical role of the small transverse free surface slope $\partial\zeta/\partial y$ is to eliminate any vertically integrated transverse flow of water. The strength of the buoyancy-driven transverse flow $v^{(1)}$ is given by

$$v^{(1)} = \frac{\alpha g H^2}{k\ u_*}\frac{\partial c^{(0)}}{\partial y}\frac{\sqrt{3}}{12}I(\varepsilon), \tag{5.4a}$$

where

$$I(\varepsilon) = \frac{(2-\varepsilon^2)(8+2\varepsilon^2+3\varepsilon^3)}{2(8+12\varepsilon-8\varepsilon^2-9\varepsilon^3+5\varepsilon^4+3\varepsilon^5)}. \tag{5.4b}$$

In view of the truncation (2.6*b*) of $\Phi^{(1)}$, these formulae (5.4*a*,*b*) are valid only to order ε. However, in a test of the usefulness of the truncated equations (3.1), (3.3*a*-*d*), (3.4*a*,*b*) it is appropriate to use the full expression (5.4*a*,*b*) and not merely the leading terms

$$I(\varepsilon) = 1 - \varepsilon\tfrac{3}{2} + \ldots. \tag{5.4c}$$

For the buoyancy-driven transverse dispersion in open-channel flow Smith (1979) derives the velocity profile

$$v(x,y,\sigma,t) = \frac{\alpha g H^2}{k\ u_*}\frac{\partial c^{(0)}}{\partial y}\frac{1}{4}\left\{2\sigma - 1 - \frac{\varepsilon}{1-\varepsilon}[1+\ln(\sigma+\sigma_*)]\right\}. \tag{5.5}$$

Figure 1 compares the dimensionless velocity profiles

$$\left\{2\sigma - 1 - \frac{\varepsilon}{1-\varepsilon}[1+\ln(\sigma+\sigma_*)]\right\} \quad \text{and} \quad I(\varepsilon)\left\{\frac{\varepsilon\Phi^{(0)}(\sigma)}{[2-\varepsilon^2]} + \frac{\Phi^{(1)}(\sigma)}{\sqrt{3}}\right\}, \tag{5.6a,b}$$

for $\varepsilon = 1/9$ and with $\Phi^{(0)}$, $\Phi^{(1)}$ as given by the truncated formulae (2.6*a*,*b*).

For the velocity profile (5.5) the corresponding transverse centroid displacement function is

$$G_\perp(\sigma) = \frac{\alpha g H^3}{8k^2u_*^2}\frac{\partial c^{(0)}}{\partial y}\left\{2\sigma - 1 - 2\frac{\varepsilon}{1-\varepsilon}\sum_{j=1}^{\infty}\frac{(-1)^{j-1}(2j+1)}{j^2(j+1)^2}P_j(2\sigma-1)\right\}. \tag{5.7}$$

The transverse counterpart of the longitudinal two-mode formula (4.11) is

$$G_\perp(\sigma) = \frac{H}{2k\,u_*}\left[\varepsilon\frac{\sqrt{3}}{2}\left(1+\frac{3}{2}\varepsilon\right)v^{(0)}+v^{(1)}\right]\sqrt{3}(2\sigma-1). \tag{5.8}$$

Substituting for $v^{(0)}$ and $v^{(1)}$ from equations (5.1), (5.4*a*) we obtain the two-mode approximation

$$G_\perp(\sigma) = \frac{\alpha g H^3}{8k^2u_*^2}\frac{\partial c^{(0)}}{\partial y}\,I(\varepsilon)\left[\frac{3\varepsilon^2(2+3\varepsilon)}{4(2-\varepsilon^2)}+1\right](2\sigma-1). \tag{5.9}$$

Figure 2 compares the shapes of the exact and approximate centroid displacement functions. Again, we emphasize that standard shear dispersion models omit this dependence upon discharge height and observation height.

For the transverse shear dispersion coefficient Smith (1979, equation (14*c*)) obtains the result

$$D_\perp = \frac{\alpha^2g^2H^5}{96k^3u_*^3}\left(\frac{\partial c^{(0)}}{\partial y}\right)^2\left[1-\frac{3\varepsilon}{1-\varepsilon}+2.42466\left(\frac{\varepsilon}{1-\varepsilon}\right)^2\right], \tag{5.10}$$

which agrees well with experimental results of Prych (1970). The transverse counterpart of the longitudinal two-mode formula (4.14) is

$$D_\perp = \left[\varepsilon\frac{\sqrt{3}}{2}\left(1+\varepsilon\tfrac{3}{2}\right)v^{(0)}+v^{(1)}\right]^2\frac{H}{2k\,u_*}. \tag{5.11}$$

Substituting for $v^{(0)}$ and $v^{(1)}$ we obtain

$$D_\perp = \frac{\alpha^2g^2H^5}{96k^3u_*^3}\left(\frac{\partial c^{(0)}}{\partial y}\right)^2 I(\varepsilon)\left\{1+\frac{3\varepsilon^2[2+3\varepsilon]}{4[2-\varepsilon^2]}\right\}^2. \tag{5.12}$$

Fortuitously, the leading numerical coefficient in the limit as ε tends to zero is the same in the exact and approximate results (5.10), (5.12). However, for $\varepsilon = 1/9$ the two-mode formula (5.12) is a factor 1.17 larger than the exact result (5.10). Thus, in buoyancy-dominated regimes the plume width would be exaggerated by about 8.5% and the peak concentrations under-predicted by about the same percentage.

6. Getting the turbulence model wrong

In a numerical implementation of the two-mode model the vertical profiles of ν and κ may vary with x, y, t and would depend upon the choice of turbulence model (Hutton, Smith & Hickmott 1987). As a measure of how well the two-mode model copes with shapes different from the reference shapes (2.2), we investigate the longitudinal flow and longitudinal dispersion for the solvable case.

$$\nu = \kappa = k\,u_*H(1-\sigma/2)(\sigma+\sigma_*). \tag{6.1}$$

The decomposition (3.2) yields the values

$$N = k\,u_*H\frac{(1-\varepsilon/2}{(1-\varepsilon)},\quad \nu' = \frac{kHu_*(\sigma+\sigma_*)(\sigma-\varepsilon)}{2(1-\varepsilon)}. \tag{6.2a,b}$$

Hence, ν' is extremely small close to the bed, but grows to twice the maximum value of the standard viscosity model (4.1*a*) near the free surface.

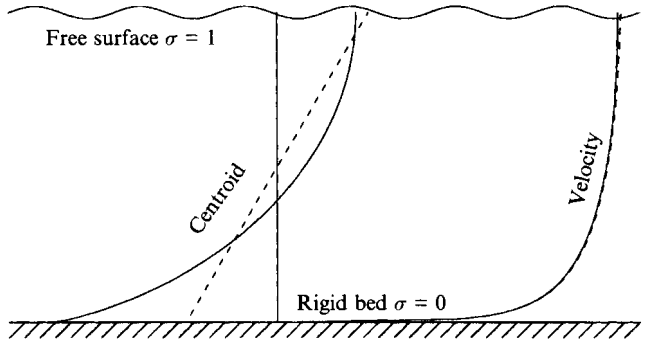

FIGURE 3. Exact results (——) for the modified logarithmic velocity profile and the corresponding centroid displacement function, compared with the two-mode approximations (- - - -).

For steady uni-directional pressure-driven flow with no buoyancy or rotation effects, the exact velocity is a modified logarithmic profile:

$$u = -\frac{H}{\varepsilon k\, u_*}\left\{\frac{1}{\rho_0}\frac{\partial P}{\partial x} + g\frac{\partial \zeta}{\partial x}\right\}\left[1 + \varepsilon \ln(\sigma + \sigma_*) + \varepsilon \ln(1 - \sigma/2)\right]. \tag{6.3}$$

With all the v' integrals evaluated explicitly, the corresponding simplifications of the two-mode momentum equations (3.3*a*,*c*) are

$$0 = -\left[1 - \frac{\varepsilon^2}{2}\right] H\left\{\frac{1}{\rho_0}\frac{\partial P}{\partial x} + g\frac{\partial \zeta}{\partial x}\right\} - \varepsilon[1 + \varepsilon]\,\frac{(1 - \varepsilon/2)}{(1 - \varepsilon)} k\, u_* u^{(0)}$$

$$-\frac{\varepsilon\sqrt{3}(1 - \varepsilon/2)}{2\,(1 - \varepsilon)} k\, u_* u^{(1)}, \tag{6.4a}$$

$$0 = \varepsilon\frac{\sqrt{3}}{2} H\left\{\frac{1}{\rho_0}\frac{\partial P}{\partial x} + g\frac{\partial \zeta}{\partial x}\right\} - \varepsilon\,\frac{\sqrt{3}(1 - \varepsilon/2)}{2(1 - \varepsilon)} k\, u_* u^{(0)} - \frac{(4 - 5\varepsilon^2)}{(1 - \varepsilon)} k\, u_* u^{(1)}. \tag{6.4b}$$

The solutions for $u^{(0)}$ and $u^{(1)}$ are

$$u^{(0)} = -\frac{H}{\varepsilon k\, u_*}\left\{\frac{1}{\rho_0}\frac{\partial P}{\partial x} + g\frac{\partial \zeta}{\partial x}\right\}\frac{2(1 - \varepsilon)(32 - 50\varepsilon^2 - 3\varepsilon^3 + 20\varepsilon^4)}{(2 - \varepsilon)(32 + 26\varepsilon - 37\varepsilon^2 + 40\varepsilon^3)}, \tag{6.5a}$$

$$u^{(1)} = \frac{H}{\varepsilon k\, u_*}\left\{\frac{1}{\rho_0}\frac{\partial P}{\partial x} + g\frac{\partial \zeta}{\partial x}\right\}\frac{2\varepsilon(1 - \varepsilon)(2 + 2\varepsilon + \varepsilon^2)\sqrt{3}}{(32 + 26\varepsilon - 37\varepsilon^2 + 40\varepsilon^3)}. \tag{6.5b}$$

Figure 3 compares the shapes of the exact (6.3) and two-mode velocity profiles. The error only becomes perceptible close to the water surface.

For the modified logarithmic velocity profile (6.3) the exact result for the asymptotic centroid velocity is

$$\bar{u} = -\frac{H}{\varepsilon k\, u_*}\left\{\frac{1}{\rho_0}\frac{\partial P}{\partial x} + g\frac{\partial \zeta}{\partial x}\right\}[1 - \varepsilon(2 - \ln 2)]. \tag{6.6}$$

With the results (6.5*a*,*b*) for $u^{(0)}$ and $u^{(1)}$, the formula (4.8) for the two-mode centroid velocity becomes

$$-\frac{H}{\varepsilon k\, u_*}\left\{\frac{1}{\rho_0}\frac{\partial P}{\partial x} + g\frac{\partial \zeta}{\partial x}\right\}\frac{2(1 - \varepsilon)(32 - 60\varepsilon^2 + 45\varepsilon^4 - 10\varepsilon^6)}{(2 - \varepsilon)(32 + 26\varepsilon - 37\varepsilon^2 + 40\varepsilon^3)}. \tag{6.7}$$

Although the fractional disparity between equations (6.6) and (6.7) is formally of order ε, the fractional error has the small value 0.0018 for $\varepsilon = 1/9$.

Correct to order σ_*, the centroid displacement function for the diffusion model (6.1) is

$$G = \frac{H^2}{k^2 u_*^2}\left\{\frac{1}{\rho_0}\frac{\partial P}{\partial x} + g\frac{\partial \zeta}{\partial x}\right\} 2\left[\ln(\sigma+\sigma_*)\ln\left(1-\frac{\sigma}{2}\right) - \ln 2 \ln\left(1-\frac{\sigma}{2}\right) - 2 + \frac{\pi^2}{6}\right]. \tag{6.8}$$

The changed formula (6.1) for κ doubles the final κ-integral in equation (3.4*b*) and halves the expression (4.11) for the approximate centroid displacement:

$$G = \frac{H}{4ku_*}\left[\varepsilon\frac{\sqrt{3}}{2}\left(1+\tfrac{3}{2}\varepsilon\right)u^{(0)} + u^{(1)}\right]\sqrt{3}(2\sigma - 1). \tag{6.9}$$

Figure 3 compares the shapes of the exact and approximate centroid displacements. The large disparities can be attributed to there only being a single mode $\Psi^{(1)}(\sigma)$ contributing to the approximation. Moreover, that single mode is not designed to accommodate the different diffusivity profile (6.1).

The exact longitudinal shear dispersion coefficient is

$$D = 0.19619\left(\frac{H}{k\,u_*}\right)^3\left\{\frac{1}{\rho_0}\frac{\partial P}{\partial x} + g\frac{\partial \zeta}{\partial x}\right\}^2. \tag{6.10}$$

Again, the changed formula (6.1) from κ halves the expression (4.14) for the approximate shear dispersion coefficient:

$$D = \left[\varepsilon\frac{\sqrt{\varepsilon}}{2}\left(1+\frac{3}{2}\varepsilon\right)u^{(0)} + u^{(1)}\right]^2\frac{H}{2k\,u_*}. \tag{6.11}$$

For $\varepsilon = 1/9$ and with the solutions (6.5*a*,*b*) for $u^{(0)}$ and $u^{(1)}$, we obtain

$$D = 0.2216\left(\frac{H}{k\,u_*}\right)^3\left\{\frac{1}{\rho_0}\frac{\partial P}{\partial x} + g\frac{\partial \zeta}{\partial x}\right\}^2. \tag{6.12}$$

Hence, there is a 1/8 over-estimate of the shear dispersion (resulting in a 1/16 under-estimate of the peak concentration). If the two-mode model had made no allowances for the disparity between the shapes of ν, κ and the initial idealization (2.2), then the numerical factor in the dispersion coefficient would have remained at the value 0.3719 (almost double the exact value).

7. Concluding remarks

When two modes $\Phi^{(0)}$, $\Phi^{(1)}$ contribute, the accuracy in replicating the velocity is impressive. For the design case with the reference eddy viscosity profile (4.1*a*) the maximum fractional error for the longitudinal velocity is 0.002 (figure 1). Even when the turbulence model (4.1*a*) is inappropriate, the maximum fractional error only increases to 0.005 (figure 3). By contrast, when there is just a single mode $\Psi^{(1)}$ to approximate different centroid displacement functions in a range of circumstances (as in figures 2 and 3) the errors are much larger. The value of the eventual shear dispersion coefficient is linked to the amplitude of that single mode. In the worst case (6.10) the shear dispersion coefficient has deviated by more than a factor of two from the reference situation (4.13). Yet, the two-mode model (6.12) still manages to get to within 0.13 of the exact result.

The referees of Part 1 posed questions, some of which are answered here.

REFERENCES

CHATWIN, P. C. 1970 The approach to normality of the concentration distribution of a solute in solvent flowing along a pipe. *J. Fluid Mech.* **43**, 321–352.

DAVIES, A. M. 1987 Spectral models in continental shelf sea oceanography. *Three-dimensional Coastal Ocean Models* (ed. N. S. Heaps), pp. 71–106. AGU.

ELDER, J. W. 1959 The dispersion of marked fluid in turbulent shear flow. *J. Fluid. Mech.* **5**, 544–560.

FALCONER, R. A. 1976 Mathematical modelling of jet-forced circulation in reservoirs and harbours. PhD thesis, Imperial College, London, 237pp.

FISCHER, H. B. 1973 Longitudinal dispersion and turbulent mixing in open-channel flow. *Ann. Rev. Fluid Mech.* **5**, 59–78.

HEAPS, N. S. 1972 On the numerical solution of the three-dimensional hydrodynamical equations for tides and storm surges. *Mem. Soc. Sci. Liege. Ser. 6*, **2**, 143–180.

HUTTON, A. G., SMITH, R. M. & HICKMOTT, S. 1987 The computation of turbulent flows of industrial complexity by the finite element method - progess and prospects. *Finite Element in Fluids* **7**, 289–309.

LAMB, H. 1945 *Hydrodynamics.* Cambridge University Press, 738pp.

PHILLIPS, N. A. 1957 A coordinate system having some special advantages for numerical forecasting. *J. Met.* **14**, 184–186.

PRYCH, E. A. 1970 Effect of density differences on lateral mixing in open-channel flow. *Keck. Lab. Hydraul. Water Res. Calif. Inst. Tech. Rep.* KH-R-21.

SMITH, R. 1979 Buoyancy effects upon lateral dispersion in open-channel flow. *J. Fluid. Mech.* **90**, 761–779.

SMITH, R. 1982 Non-uniform discharges of contaminants in shear flows. *J. Fluid mech.* **120**, 71–89.

SMITH, R. 1995 Multi-mode models of flow and of solute dispersion in shallow water. Part 1. General derivation. *J. Fluid Mech.* (in the press).

TAYLOR, G. I. 1953 Dispersion of soluble matter in solvent flowing slowly through a tube. *Proc. R. Soc. Lond.* A **219**, 186–203.